Point Charge Distributions and Electrostatic Steering in Enzyme/Substrate Encounter: Brownian Dynamics of Modified Copper/Zinc Superoxide Dismutases†

Jacqueline J. Sines* and Stuart A. Allison
Department of Chemistry, Georgia State University, Atlanta, Georgia 30303
J. Andrew McCammon
Department of Chemistry, University of Houston, Houston, Texas 77204-5641
Received October 4, 1989; Revised Manuscript Received July 12, 1990

ABSTRACT: The electrostatic steering mechanism of bovine erythrocyte Cu/Zn superoxide dismutase (SOD) was investigated through the use of Brownian dynamics. Simulations of enzyme/substrate encounter were carried out on 14 different SOD models defined by simple changes in the enzyme's point charge distribution. The magnitude and ionic strength dependence of reaction rates, rates for collision anywhere on the enzyme surface, and collision efficiency factors were analyzed to elucidate both the general and specific roles for point charges associated with amino acid residues. Collision rates for the general enzyme surface appear to be solely determined by the net charge on the enzyme. At physiological ionic strength this effect is negligible, with only 6% variation in collision rates observed as the net charge ranges from +2e to −10e. With the exception of a few charged residues in the active-site channel of SOD, point charge modifications had modest effects on reaction rates. For a large region within and surrounding the channel, reaction rates increased or decreased by only 10–15% with the addition or subtraction of a protonic unit of charge, respectively. This effect simply disappeared with increasing distance from the active site. More dramatic effects were seen at only three residues: arginine-141, glutamate-131, and lysine-134. Implications for rate enhancement through site-directed mutagenesis are discussed.

The diffusion of a charged substrate molecule to the active site of an enzyme is greatly affected by electrostatic interactions between substrate and charged amino acid residues (Neumann, 1981; Case, 1988). Two types of effects are possible: the enzyme charge distribution may influence the nonspecific collision rate for substrate encounter with any part of the enzyme surface or it may steer substrate to a particular area of the enzyme surface, altering the probability that an enzyme–substrate complex will result from collision. This is reflected in the empirical equation for the bimolecular reaction rate constant

$$k = k_c P \exp(-E_{act}/RT) = k_c P Z \qquad (1)$$

where k_c and P represent the bimolecular rate constant for nonspecific collisions and a collision efficiency factor, respectively, and Z is an energy factor for the reaction. When enzyme catalytic rates approach diffusion-controlled limits, $E_{act} \approx 0$, so that $Z \approx 1$ and k_c and P determine the reaction rate. In such cases, P is simply the ratio of k to k_c, equal to the conditional probability of reaction, given that collision has occurred. In the absence of electrostatic interactions between enzyme and substrate, P is determined by the surface topography of the enzyme. The change induced in this base-line P by the presence of electrostatic forces is a measure of the effectiveness of electrostatic steering.

To understand the electrostatics of enzyme catalysis, it is necessary to investigate the effects of individual charged amino acid residues on both collision rate and collision efficiency. Although experimental approaches that modify or replace residues are essential in this regard, difficulties in distinguishing the two factors and the possibility of effects secondary to the charge alteration may complicate the interpretation. Alternative theoretical treatments are complicated by irregularities of enzyme shape and charge distribution. This complexity has prevented analytical solution of the enzyme/substrate encounter problem, but numerical solution is possible, using Brownian dynamics simulations (Northrup et al., 1984). In this method, Brownian motion is explicitly modeled by using a computer representation of the system of interest. The most detailed models use the linearized (Sharp et al., 1987a,b; Allison et al., 1988; Sines et al., 1990) or full (Allison et al., 1989; Jayaram et al., 1989) Poisson–Boltzmann equation to account for electrostatic forces (Davis & McCammon, 1990).

Bovine erythrocyte Cu/Zn superoxide dismutase has been the prototype for the development of Brownian dynamics applications to enzyme–substrate systems (Allison & McCammon, 1985; Allison et al., 1985, 1986, 1988, 1989; Ganti et al., 1985; Sharp et al., 1987a,b; Head-Gordon & Brooks, 1987) and is the subject of this study. Superoxide dismutases (SOD's) constitute a class of enymes (EC 1.15.1.1) that catalyze the dismutation of the superoxide anion radical [see Halliwell and Gutteridge (1984), Fridovich (1986), and Bannister et al. (1987) for a comprehensive review]. Regardless of source, catalysis by SOD appears to proceed by a minimal mechanism involving cyclical oxidation/reduction of a metal cofactor. For Cu/Zn SOD's, the conventional kinetic scheme (Klug-Roth et al., 1973; Fielden et al., 1974) is described by

$$\text{E–Cu}^{2+} + {}^{\bullet}O_2^- \rightarrow \text{E–Cu}^{+} + O_2$$

$$\text{E–Cu}^{+} + {}^{\bullet}O_2^- + 2H^+ \rightarrow \text{E–Cu}^{2+} + H_2O_2$$

$$\text{net} \quad 2{}^{\bullet}O_2^- + 2H^+ \xrightarrow{\text{SOD}} O_2 + H_2O_2 \qquad (2)$$

† Supported in part by the NSF and, at the University of Houston, by the NIH, the Robert A. Welch Foundation, and the Texas Advanced Research Program. S.A.A. is the recipient of a Presidential Young Investigatorship Award. J.A.M. is the recipient of the George H. Hitchings Award from the Burroughs Wellcome Fund.

* Address correspondence to this author at the Department of Chemistry, University of Houston Texas, Houston, TX 77204-5641.

0006-2960/90/0429-9403$02.50/0

although more complex mechanisms (Osman & Basch, 1984) have been suggested. The reaction is extremely rapid, with a bimolecular rate constant for either step on the order of 10^9 M^{-1} s^{-1} (Klug-Roth et al., 1973; Fielden et al., 1974; Malinowski & Fridovich, 1979), in the range of typical diffusion-controlled reactions. Indication of electrostatic steering is seen in the unusual salt dependence of the reaction rate. Most SOD's, including the bovine erythrocyte enzyme with its net charge of about −4e, are negatively charged, as is superoxide. The rate of the reaction, however, decreases with increasing salt, except perhaps for salt concentrations near zero (Rigo et al., 1975; Cudd & Fridovich, 1982; Argese et al., 1987; O'Neill et al., 1988). Simple diffusion models predict the opposite behavior for encounter of like-charged ions (Debye, 1942), since increased ion screening should decrease electrostatic repulsion and thereby increase encounter rates. More detailed electrostatic models incorporating the complex charge distribution of the enzyme (Koppenol, 1981; Getzoff et al., 1983; Klapper et al., 1986) can account for the observed negative salt dependence through the effect of solvent ions on electrostatic steering.

In previous SOD Brownian dynamics simulations using linearized Poisson–Boltzmann potentials, calculated bimolecular diffusional rate constants were only 2-fold higher than experimental values (Allison et al., 1988) and exhibited the observed negative ionic strength dependence (Sharp et al., 1987a,b; Allison et al., 1988). This work reports on further application of this technique to SOD catalysis, addressing the role of individual point charges in electrostatic facilitation of the reaction. From these simulations, we extract not only bimolecular diffusional rate constants for reaction (superoxide encounter with the active site copper) as in previous work but also rate constants for collision (encounter of superoxide anywhere on the enzyme surface). The ratio of these rate constants defines the collision efficiency factor, $P = k/k_c$ of eq 1, the probability that a collision between superoxide and SOD will be effective. For each model, simulations have been conducted at a range of ionic strength including physiological salt ($I = \sim 0.15$ M), using the salt dependence of P as a probe for electrostatic steering.

We have simulated the encounter of superoxide with "wild-type" Cu/Zn SOD and with various modified SOD's defined by simple changes in the point charge distribution of the enzyme. This approach for defining modified enzyme molecules was chosen to address purely electrostatic effects of possible alterations in the SOD primary structure. More detailed modeling could include actual residue substitution, but local structural changes (Matthews, 1987, and references therein) might mask the effect of the charge modification itself. Since we are concentrating on diffusional encounter, post-diffusional kinetic effects of amino acid modifications are also ignored in our simulations. Our results are thus not expected to correspond completely with experimental rate measurements of mutated or derivatized SOD's. Instead, the simplified model system that we use isolates the specific effects of charge substitution on the diffusional process. In this way, we hope to understand features of electrostatic steering mechanisms that might be obscured in a more complete model.

Methods

The Brownian dynamics method used in this work is similar to that used previously (Allison et al., 1988). The 2-Å resolution crystal structure of the Cu/Zn SOD homodimer (Tainer et al., 1982) is superimposed upon a three-dimensional Cartesian grid. Lattice points, at 1-Å resolution, are assigned reactivity and solute exclusion criteria for Brownian dynamics simulations. Concentric spheres are defined at radii $b = 41.5$ Å and $q = 500$ Å from the SOD center of charge.[1] Each simulation consists of a series of superoxide trajectories, which are initiated at sphere b and terminated when superoxide encounters the reactive copper cofactor or diffuses past sphere q. We have chosen b and q so that simulation results are independent of small changes in their values. For all models except wild type (where greater precision was desired for other studies), we ran 12 000 trajectories to calculate the reported rates, obtaining relative standard deviations less than 1%, based on batched of 500 trajectories. The probability of reaction within such a truncated trajectory, β_{rxn}, is simply the number of superoxide–copper collisions, n_{rxn}, divided by the total number of trajectories, n_{traj}. We also keep track of the number of trajectories, n_{0col}, that terminate at the 500-Å sphere with no encounter of superoxide with any atom of SOD. The probability of collision of superoxide with any atom of SOD during a truncated trajectory is then

$$\beta_{col} = 1 - (n_{0col}/n_{traj}) \quad (3)$$

The probabilities, β, for collision or reaction during truncated trajectories are converted to probabilities for hypothetical infinite trajectories, β_∞, by using (Northrup et al., 1984)

$$\beta_\infty = \beta/[1 - (1 - \beta)\Omega] \quad (4)$$

Ω is the conditional probability of reaching b, given that a point charge has reached q, and is defined by

$$\Omega = k_D(b)/k_D(q) \quad (5)$$

where $k_D(r)$ is the modified Debye rate constant for diffusion of superoxide to a sphere of radius r as discussed below. Rates for both reaction (encounter with copper) and collision (encounter anywhere on the SOD surface) are finally derived by using

$$k = k_D(b)\beta_\infty \quad (6)$$

Trajectory Propagation. Trajectories are composed of a series of small time steps, each of which is the sum of Brownian motion and electrostatic components. The evolution of $\mathbf{r}$, the position vector of superoxide relative to the grid origin, is defined by

$$\mathbf{r}(t + \Delta t) = \mathbf{r}(t) + (k_B T)^{-1} D_r \Delta t \mathbf{f}(t) + \mathbf{s} \quad (7)$$

where k_B is the Boltzmann constant, T is 298 K, D_r is the relative diffusion constant for SOD and superoxide, Δt is the time step, $\mathbf{f} = -\nabla U$ is the electrostatic force on superoxide (with U representing the potential), and $\mathbf{s}$ is a vector of independent Gaussian random numbers with $\langle s \rangle = 0$ and $\langle s^2 \rangle = 2D_r\Delta t$ for x, y, and z components. $D_r = 0.1283$ Å^2/ps is the sum of translational diffusion constants for superoxide and SOD, based on hydrodynamic radii of 2.05 and 28.5 Å, respectively, and stick boundary conditions. When substrate is far from the enzyme, Debye–Hückel potentials (see below) based on the net enzyme charge and a finite ion radius of 30 Å are used to generate electrostatic forces (Northrup et al., 1984). Close to the enzyme, the effect of the complex charge distribution is taken into account through the use of linearized Poisson–Boltzmann potentials.

Linearized Poisson–Boltzmann Potentials. Charges are assigned to amino acid residues and metal ligands for the purpose of calculating the electrostatic potential (Allison et

[1] The center of charge of the SOD dimer is defined by using $\sum_i \mathbf{r}_i|z_i| = 0$, where $\mathbf{r}_i$ is the vector from the center of charge to charge i, z_i is the charge on charge i, and the summation is over the charge distribution of the wild-type enzyme.

al., 1985). For unmodified SOD single point charges of +1e or −1e are assigned to lysine and arginine or glutamate and aspartate residues, respectively. The carboxy terminal has a −1e charge while the amino terminal is neutral due to acetylation. Histidine-41 is assigned a charge of +1e due to its apparent role as a proton donor in two H bonds and histidine-61 has a charge of −1e because it is ligated to both copper and zinc ions [see Getzoff et al. (1983) for further discussion]. All other histidines are neutral.[2] Copper and zinc ligands are assigned charges of +2e. These 76 charge assignments for the SOD dimer yield a net enzyme charge of −4e. In numerous test simulations, this simple charge distribution yielded results indistinguishable from models using partial charge assignments on all enzyme atoms (Allison et al., 1986, and unpublished observations).

For modified enzyme studies, the crystal structure of wild-type SOD is retained; modifications are defined as simple changes in point charges associated with residues or ligands. Where such residues or ligands are charged in the unmodified model, charge coordinates are retained. In cases where neutral residues are assigned charges, we use the CB coordinates for all residues except asparagine, in which case CG coordinates are used. These carbons correspond to the only side-chain carbon of alanine and the carbons at which branching of the side chain occurs for the other residues. We initially chose these charge positions to minimize any effects due to differences in side-chain structures. However, simulated rates prove to be relatively insensitive to small changes in charge coordinates so that any charge position within the side chains would have yielded essentially identical results.

The enzyme representation is positioned within a Cartesian grid at 1-Å resolution. The center of charge for the wild-type enzyme is aligned with the center of a 100 × 100 × 100 Å^3 grid, which we define as the grid origin. Since one face of this grid cube was considerably closer to the enzyme surface than the others, we added an additional 4 Å to the grid in this direction, yielding a final grid size of 100 × 100 × 104 Å. By running simulations with larger and smaller grids on numerous test models, we have determined that this grid size is large enough to eliminate the effects from the potential discontinuity at the grid boundary. Lattice points, at 1-Å resolution, are assigned point charge values by using a trilinear weighting function (Edmunds et al., 1984). All grid points falling within the SOD dimer representation have a dielectric of 2, while a value of 78 is used for remaining solvent grid points. Grid boundary potentials are calculated by using Debye–Hückel theory based on a finite ion radius of 30 Å and the net enzyme charge for the model under study (Northrup et al., 1984). The linearized Poisson–Boltzmann equation is solved for interior grid points by using a finite difference method that takes into consideration these charges, dielectric constants, and boundary potentials (Allison et al., 1988; Warwicker & Watson, 1982; Edmonds et al., 1984; Rogers & Sternberg, 1984; Klapper et al., 1986).

Modified Debye Model. Rate constants for diffusion of superoxide toward uniformly reactive charged spheres [k_D(a)] are used in eq 5 and 6 and for comparison of collision rates for superoxide with SOD versus a 28-Å sphere (Figures 1 and 3). These rates are based on a model that accounts for electrostatic interactions through the use of Debye–Hückel potentials. The relevant equation (Northrup & Hynes, 1979) for diffusion to a sphere of radius a is

$$k_D(a) = 4\pi D_r / \int_a^\infty r^{-2} \exp[U(r)/k_B T]\, dr \qquad (8)$$

where $U(r)/k_BT$ is the potential at distance r from the center of the sphere in units of k_BT and is given by

$$U(r)/k_BT = c \exp(-\kappa r)/r \qquad (9)$$

The constant c is

$$c = q_1 q_2 e^2 \exp(\kappa r)/\epsilon k_B T(1 + \kappa r_0) \qquad (10)$$

κ is the Debye screening parameter, r_0 is the finite ion radius (equal to 30 Å for purposes of eq 5 and 6 and 28 Å for Figures 1 and 3), $q_1q_2e^2$ is the product of net charges on superoxide and SOD, and $\epsilon = 78$, the dielectric constant of the medium. For monovalent added salt at ionic strength I (moles per liter) and 25 °C (Dickerson, 1969)

$$\kappa = 0.329 I^{1/2}\ \text{Å}^{-1} \qquad (11)$$

Technical Details. Brownian dynamics simulations and calculations of linearized Poisson–Boltzmann potentials were performed in single precision on an Amdahl 5860 or an Amdahl 5880. Extensive testing at double precision revealed no significant differences in results with the models and methods used here. The simulation parameters used in our previous work (Allison et al., 1988) were subjected to rigorous reevaluation by using the models of the current work. Only several modifications were required for the less well-behaved models sometimes produced when we modified the charge distribution. The reaction radius of copper, r^*, is used to define termination of a trajectory in reaction. In our previous work, we used r^* = 4.0 Å, which is somewhat larger than the sum of the van der Waals radii of copper and superoxide but was the minimum value for which reaction rates for the two sites were equivalent. With the fairly major alterations in electrostatic potential around the active sites in some models, it was necessary to increase r^* to 4.5 Å for greater site equivalency. We have used this value in all of the simulations reported here. In addition, at low salt and with larger absolute values of the net SOD charge, we have found it necessary to used a stricter criterion for convergence of the finite difference iterations during computation of the linearized Poisson–Boltzmann potentials. In previous work (Allison et al., 1988) convergence was assumed when

$$\sum_{ijk}[U_{ijk}^{(s+1)} - U_{ijk}^{(s)}]^2 / \sum_{ijk}[U_{ijk}^{(s+1)}]^2 < 10^{-6} \qquad (12)$$

where $U_{ijk}^{(s)}$ represents the electrostatic potential at lattice site i,j,k after iteration number s. (Equations 9 and 11 in Allison et al. (1988) and Allison et al. (1989), respectively, are missing a summation sign in the denominator. These are typographical errors.) We employ here instead a tolerance of 10^{-8} or 10^{-9} at low salt for all models and at all salt for many of the models that have gross alterations in the active-site charge distribution.

The greater size and finer resolution of the potential grid, as well as stricter convergence criteria, tend to greatly increase cpu requirements in comparison to previous work. Offsetting these increases are various changes in algorithms, which increased computational efficiency without affecting simulation results. One noteworthy program change was the calculation of forces within the potential grid during trajectory propa-

[2] Histidine-19 appears to have a pK_a of 6.7 (Cass et al., 1977). This charge model thus applies most directly to the SOD protonation state at pH's somewhat above neutrality. (At pH 8, ~90% of SOD dimers would have both histidine-19 residues protonated.) However, our present results suggest that a 1e point charge at one or both His-19's, distant from the active site, would have little effect on rates. (See threonine-17 in Figure 8.) This is also suggested by experimental results showing constant SOD activity in a pH range of 5–10 (Cudd & Fridovich, 1982; Argese et al., 1987). Future simulations will address other protonation states of the enzyme.

gation, rather than prior calculation and storage in a 3-fold larger array. At high salt (I = 0.437 M) cpu times are relatively model independent. By use of a tolerance of 10^{-9} (eq 12) and a relaxation parameter of 1.5, calculation of the potential grid is accomplished in about 6–8 cpu min, while the simulation routine requires ~2.2–2.3 min for each 1000 trajectories. At lower ionic strength (where the magnitude of the potential is greater and convergence therefore is expected to take more iterations) considerable model-to-model variation in cpu demands is observed. For wild-type SOD at I = 0.005 M, calculation of the electrostatic potential grid requires 39 cpu min and 1000 trajectories are completed in ~1.7 cpu min. Models in which three positive or negative charges are added to each active-site region (Table I), yielding net enzyme charges of +2e or −10e, respectively, converge much more slowly during the finite difference iterations of the potential calculation. The former model requires 50 cpu min for the grid calculation while the latter requires 72 min. Cpu times for 1000 trajectories in the two cases are ~2.0 and ~1.3 min, respectively.

The integration in eq 8 is solved on a Microvax II using the DQDAG function in Version 10 of the IMSL Math Library. Numerical integration is performed in double precision by using a Gauss–Kronrod rule in subdivided intervals, with error estimation by a Gauss quadrature rule.

Results and Discussion

Oxidized SOD Form. Simulations on wild-type Cu/Zn SOD yielded reaction rate constants (solid line in Figure 1a) with negative ionic strength dependence, in agreement with experimental observation (Rigo et al., 1975; Cudd & Fridovich, 1982; Argese et al., 1987; O'Neill et al., 1988). These reaction rates are less than collision rates (dashed line), since reaction requires encounter of superoxide and Cu^{2+}, while collision occurs when superoxide encounters any part of the enzyme molecule. In contrast to reaction rates, collision rates exhibit a positive ionic strength dependence, characteristic of simple encounter of like-charged species. The dotted line in Figure 1a corresponds to a modified Debye model for encounter of a −1e point charge and a uniformly reactive 28-Å sphere with a central charge equal to −4e, the net SOD charge. The correspondence of collision rates with the modified Debye model is striking. Although the rate magnitudes for the Debye model are sensitive to the reaction radius of the sphere, the ionic strength dependence is similar for any radius chosen.

Our simulated reaction rates reflect this positive ionic strength dependence of collision rates (indicative of repulsive interaction) as well as attractive electrostatic steering effects. The derived variable $P = k/k_c$, which is the probability that a collision between superoxide and SOD will be catalytically effective, should be a more direct indicator of salt effects upon the steering mechanism of SOD. As expected, the negative ionic strength dependence of P (Figure 1b) is more pronounced than that seen for reaction rates, since the collision rate in the denominator of the ratio exhibits positive salt dependence. For wild-type SOD we find that the values of P vary from about 35% [log (P) ≈ −0.5] to about 10% [log (P) ≈ −1] as ionic strength is increased from 0.005 to 0.437 M (Figure 1b). The value of P at high salt, that is with maximum ion shielding, agrees with rough estimates of Cu/Zn SOD effectiveness, calculated as the ratio of experimentally observed rates to a simple Debye–Smoluchowski neutral-sphere model (Koppenol, 1981). For comparative purposes, we ran simulations without electrostatic forces, that is where reaction rates are determined solely by random Brownian motion. In such simulations, P values are about 1.6%. The 10–35% values of P from wild-type

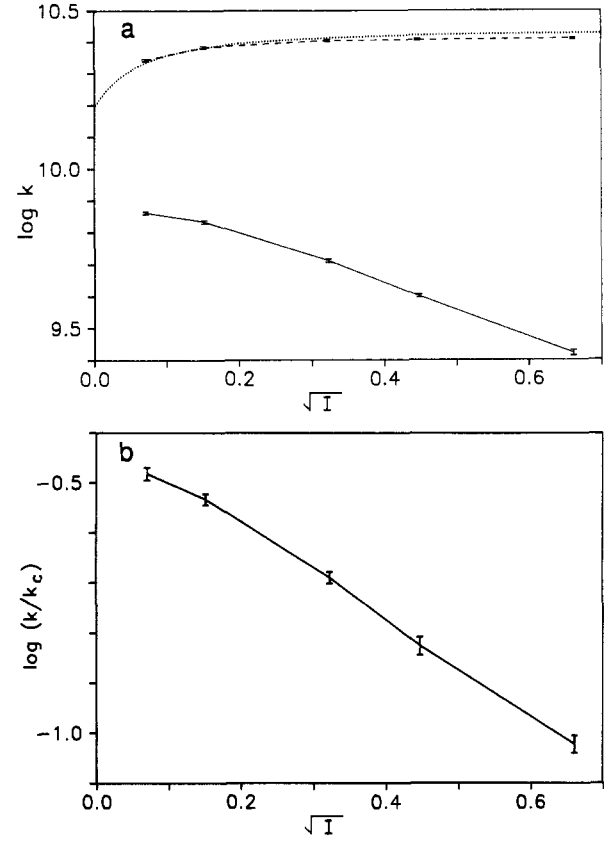

FIGURE 1: Simulation results for wild-type SOD. Points resulting from simulations are indicated by error bars (standard deviation). At each salt concentration, reaction rates are the result of 48 000 trajectories while for collision rates and collision efficiencies 12 000 trajectories were used. (a) Solid and dashed lines indicate bimolecular rate constants for reaction and collision, respectively. Dotted line corresponds to a modified Debye model for superoxide encounter with a uniformly reactive sphere of radius 28 Å and central charge −4e as discussed in the text. In this and succeeding figures, rates are normalized to 1 M^{-1} s^{-1} and I is in units of M. Note that $I^{1/2}$ is proportional to κ, the Debye screening parameter (eq 11). (b) Collision efficiencies.

simulations therefore indicate a high degree of efficiency in the electrostatic steering mechanism of Cu/Zn SOD.

Dependence of Collision Rate on Net Charge. We investigated the possibility that the simple monopole–monopole model that fit wild-type collision rates (Figure 1a) could predict the behavior of SOD models with modified charge distributions as well. Charges associated with residues in the active site area and on the β-barrel forming the "back" side of the enzyme were increased or decreased. In Figure 2, a sketch of the active-site region of one SOD subunit combined with a portion of the β-barrel of the opposite subunit of the dimer identifies the residues that have been modified.

As discussed below and observed in further unpublished results, point charge modifications affect reaction rates in complex ways that are not simply related to the net enzyme charge. In contrast, we observe very strong correlations between net enzyme charge and rates for collision of superoxide with the general SOD surface. Representative data appear in Table I. For a given ionic strength and enzyme charge, collision rates are nearly identical within the precision of the simulations, in spite of quite different alterations in the charge distributions. Averages of the data of Table I, grouped by net charge, are plotted in Figure 3. We observe significant differences in collision rate only at low ionic strength as the net charge is varied from +2e to −10e. At physiological salt, the −4e charge on wild-type SOD results in a negligible 3%

Table I: Simulated Collision Rates for Modified SOD's and Superoxide

net charge	changes from wt	$k_c \times 10^{-10}$ M s at $I \times$ M^{-1} 0.005	0.023	0.104	0.200	0.437
+2	58, 63, 138 → +1	2.94 (0.02)	2.74 (0.02)	2.63 (0.01)	2.62 (0.02)	2.63 (0.02)
0	11 → +1	2.67 (0.01)	2.65 (0.02)	2.62 (0.02)	2.60 (0.02)	2.63 (0.02)
	130 → +1	2.69 (0.02)	2.68 (0.02)	2.66 (0.02)	2.62 (0.02)	2.65 (0.02)
	131 → +1	2.66 (0.02)	2.64 (0.02)	2.64 (0.02)	2.62 (0.02)	2.62 (0.02)
−2	11 → 0	2.42 (0.02)	2.55 (0.02)	2.57 (0.02)	2.60 (0.02)	2.63 (0.02)
	130 → 0	2.44 (0.02)	2.51 (0.01)	2.62 (0.02)	2.62 (0.02)	2.62 (0.02)
	131 → 0	2.45 (0.02)	2.52 (0.01)	2.57 (0.02)	2.63 (0.02)	2.60 (0.02)
−4	wt	2.20 (0.02)	2.42 (0.01)	2.54 (0.02)	2.55 (0.02)	2.57 (0.01)
	5 → −1, 131 → 0	2.20 (0.02)	2.39 (0.02)	2.56 (0.02)	2.57 (0.02)	2.63 (0.02)
	63 → −1, 131 → 0	2.23 (0.02)	2.44 (0.02)	2.55 (0.02)	2.57 (0.02)	2.60 (0.02)
	94 → −1, 131 → 0	2.23 (0.02)	2.40 (0.02)	2.51 (0.02)	2.55 (0.01)	2.61 (0.01)
−6	120 → 0	1.94 (0.01)	2.30 (0.02)	2.50 (0.02)	2.56 (0.02)	2.60 (0.02)
	134 → 0	1.93 (0.02)	2.28 (0.02)	2.50 (0.02)	2.56 (0.02)	2.60 (0.02)
	141 → 0	1.95 (0.02)	2.26 (0.02)	2.52 (0.02)	2.56 (0.01)	2.61 (0.02)
−8	120 → −1	1.73 (0.02)	2.15 (0.01)	2.45 (0.01)	2.54 (0.02)	2.57 (0.02)
	134 → −1	1.67 (0.02)	2.13 (0.02)	2.46 (0.02)	2.54 (0.02)	2.59 (0.02)
	141 → −1	1.69 (0.01)	2.16 (0.02)	2.49 (0.01)	2.58 (0.02)	2.64 (0.02)
−10	58, 63, 138 → −1	1.47 (0.01)	2.03 (0.02)	2.44 (0.02)	2.51 (0.01)	2.56 (0.02)

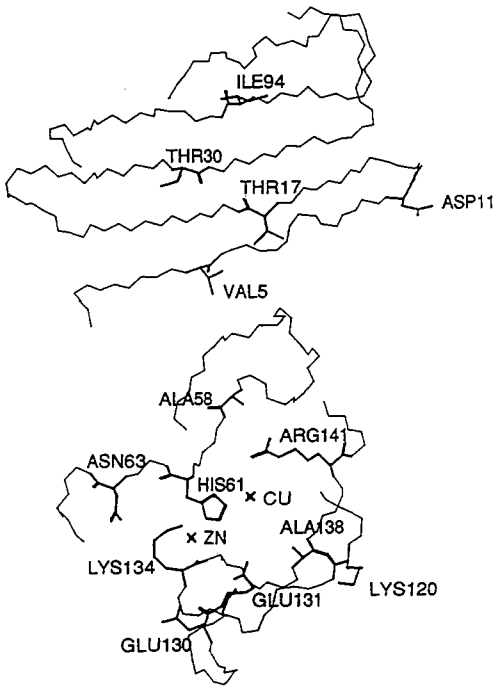

FIGURE 2: Partial structures of one active-site channel and one β-barrel portion of the Cu/Zn dimer showing SOD residues subjected to point charge modifications. Residues 5, 11, 17, 30, and 94 are on the β-barrel of one subunit, while remaining residues surround the catalytic copper of the other. The figure was generated by using Biograf molecular modeling software.

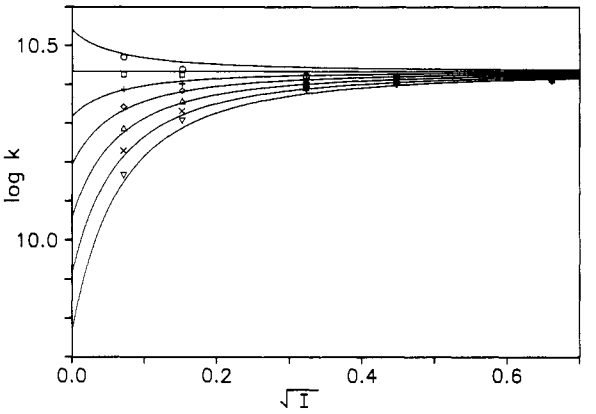

FIGURE 3: Dependence of bimolecular collision rates on net SOD charge and comparison to modified Debye models. Points represent averages of simulation results (Table I) for modified SOD's with net charges equal to +2 (○), 0 (□), −2 (+), −4 (◇), −6 (△), −8 (×), and −10 (▽) in units of protonic charge. Solid lines indicate bimolecular rate constants for superoxide encounter with uniformly reactive 28-Å spheres with central charges equal to the net charges of SOD models. (Top to bottom: +2, 0, −2, −4, −6, −8, and −10 in units of protonic charge.)

decrease in collision rate in comparison to neutral SOD models. Superimposed on the data are graphs for a modified Debye model of a uniformly reactive sphere of reaction radius 28 Å with varying central charge. The correspondence of the two types of models, detailed and spherical, is impressive. It is possible that the small deviations would disappear if a more geometrically accurate simple model, such as an ellipsoid, were used.

These results strongly suggest that long-range, monopole effects resulting from the net enzyme charge influence the diffusion of superoxide to the SOD dimer as a whole. These effects are independent of the detailed charge distribution of SOD. The highly asymmetric distribution would have its steering effects at shorter range, biasing encounters to the active site but not affecting the total rate for encounter with the enzyme surface.[3] The nearly identical catalytic behaviors of negatively charged bovine, neutral porcine, and positively charged ovine Cu/Zn SOD's (O'Neill et al., 1988) substantiate this model. The small differences in k_c expected from the differing net charges of the homologous enzymes would not be reflected in significant differences in reaction rates. Pairwise additive Coulomb potentials suggest that electrostatic steering is conserved in the three enzymes (Desideri et al., 1988), which would be reflected in similar P values in our

[3] The long-range versus short-range interactions discussed here may reflect a sharp division between effects of the enzyme's monopole moment and its higher moments. [For Cu/Zn SOD this division could be accentuated by the absence of a significant dipole moment, since a simple one-dielectric model predicts that the effects of the dipole moment are small in comparison to those of the monopole and quadrupole moments (Allison et al., 1985).] Monopole–monopole interactions fall off with the inverse of the distance between charges (R^{-1}). They would govern the approach of superoxide to a region around the enzyme where Brownian motion ensures enzyme–substrate collision. Other moments, with energies depending on higher powers of R^{-1}, would not be important in the initial approach to this "collision region" but would strongly steer substrate within it.

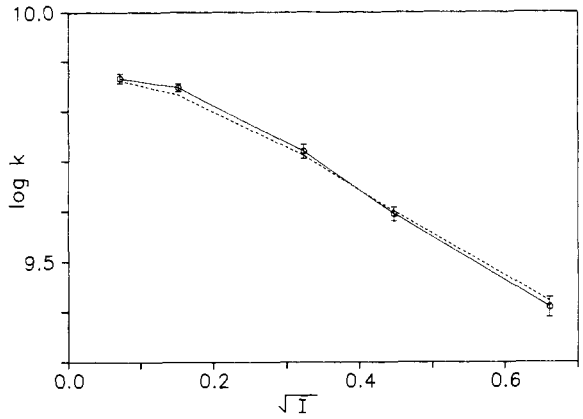

FIGURE 4: Comparison of Cu^{2+} and Cu^{+} SOD models. Dashed line corresponds to bimolecular reaction rate constants for Cu^{2+} SOD from Figure 1a. Points indicate bimolecular reaction rate constant derived from simulations on Cu^{+} SOD, with error bars representing standard deviations.

treatment. Similar reaction rates for the variously charged SOD's would thus be expected.

Reaction Rates for the Reduced SOD Form. Although the conventional mechanism for SOD catalysis (eq 1) predicts equal participation of reduced and oxidized enzyme forms in catalysis, previous Brownian dynamics simulations have modeled catalysis by Cu^{2+}–SOD only. We present here the results of simulations of Cu^{+}–SOD catalysis, using simple point charge changes to model the reduced enzyme form. For these simulations, point charges associated with the copper ligands were reduced from two units of protonic charge to one, retaining the Cu^{2+} crystal structure coordinates as discussed above. Charges associated with histidine-61 (Figure 2) were simultaneously increased to account for the proposed protonation of this residue upon SOD reduction (Hodgson & Fridovich, 1975; McAdam et al., 1977). We found no significant differences in reaction rates between the oxidized and reduced forms over the ionic strength range studied (Figure 4). This is in agreement with experimental results indicating equal rates for catalysis by Cu^{+} and Cu^{2+} enzyme forms [see Bannister et al. (1987) for a recent review].

Modification of Positively Charged Residues. Electrostatic steering of superoxide toward the catalytic copper cofactor has been attributed, at least in part, to a region of attractive potential surrounding the active-site channel of Cu/Zn SOD (Koppenol, 1981; Getzoff et al., 1983). We have selected for investigation three of the positively charged residues in the active-site region that have been hypothesized to be important in generating this potential (Malinowski & Fridovich, 1979; Cudd & Fridovich, 1982; Getzoff et al., 1983). All three residues—arginine-141, lysine-134, and lysine-120—are highly conserved in CuZn SOD's for which sequence data are available, with arginine-141 being invariant in naturally occurring enzymes [see Bannister et al. (1987), Hjalmarsson et al. (1987), and Getzoff et al. (1989) and references therein]. Their positive charges have been both neutralized and reversed to generate models with altered potential fields in hopes of defining the roles these residues play in steering superoxide for productive encounter. Simulation results are presented in Figure 5. As would be expected, both from these residues' likely involvement in short-range steering effects and from their contribution to the overall charge on SOD, we see reduced rates for all modifications, greater reductions being associated with reversal of charge in comparison to neutralization.

The greatest rate decreases are observed when we modify the charge associated with arginine-141, situated at the bottom

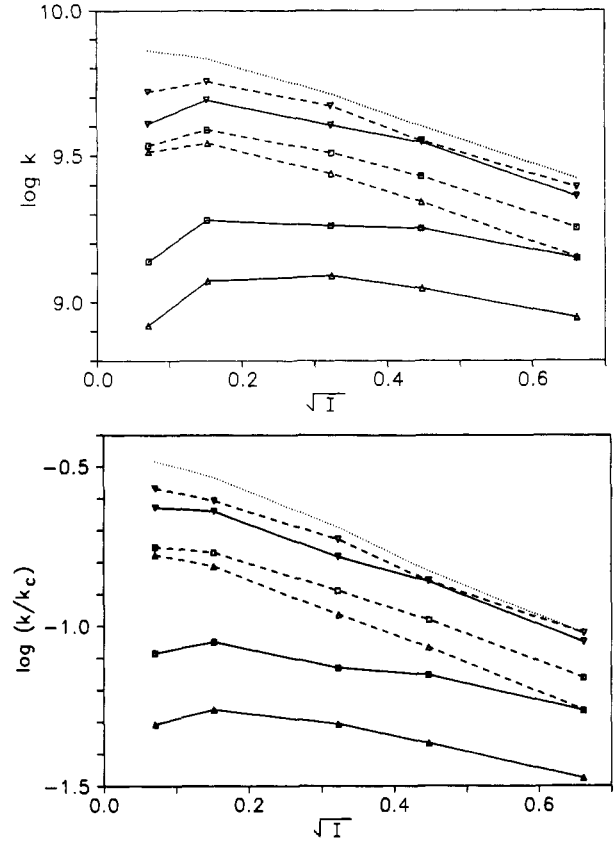

FIGURE 5: Simulations of SOD models with point charge modifications at cationic residues. Dotted lines correspond to results for wild-type SOD from Figure 1. Symbols correspond to SOD models with modifications at arginine-141 (△), lysine-134 (□), and lysine-120 (▽). Dashed and solid lines represent results from simulations in which charges were neutralized and reversed, respectively. (a) Bimolecular reaction rates. Standard deviations (not shown) are approximately equal to those for Cu^{+} SOD in Figure 4. (b) Collision efficiencies. Standard deviations (not shown) are approximately equal to those for wild-type SOD in Figure 1b.

of the active-site channel immediately adjacent to the copper ion (Figure 2). Neutralization of this residue results in simulated reaction rates that are 45–60% of wild-type rates, while a negative charge at this position reduces reaction rates to 12–33% of wild type rates. Except at low ionic strength, the ionic strength dependence of the simulated reaction is not observed to change much upon neutralization of this residue. However, it is significantly altered when the positive charge is replaced by a negative charge (Figure 5a). Sharp and co-workers (Sharp et al., 1987a) have also conducted Brownian dynamics simulations on the 141-neutralized enzyme and observed a significantly smaller effect on the magnitude of reaction rates. Although a different range of ionic strength was used in this previous study, salt dependence effects on reaction rates due to neutralization of 141 are similar within the range of overlap (I = 0.005–0.144 M) with our data (Figure 5a). Possible reasons from the discrepancy in rate magnitudes include the higher resolution and larger size of the potential grid in the current work and differences in convergence criteria during calculation of the electrostatic potential field. [While we have extensively tested for convergence, not only for the wild-type SOD model but also for altered charge distributions, which sometimes generate less well-behaved systems, it is not clear that this was done in some previous work (Klapper et al., 1986; Sharp et al., 1987a,b).]

These observed effects on reaction rates reflect both reduced efficiency of the steering mechanism due to loss of an important positive charge at arginine-141 and more general

effects due to decreases in net charge on the enzyme. Long-range monopole–monopole interactions, as reflected in gross collision rates, have been factored out of reaction rates in calculation of the collision efficiencies in Figure 5b. Neutralization of arginine-141 greatly reduces the efficiency of electrostatic steering, as collision efficiencies are reduced about 2-fold at all salt concentrations, but very little effect on salt dependency is observed. Roughly half the salt dependency of wild-type SOD collision efficiencies remains even when the charge on 141 is reversed and magnitudes of P are reduced to 15–35% of wild type.

Experiments on bovine erythrocyte Cu/Zn SOD covalently modified at arginine-141 indicate 80–98% suppression of activity accompanying neutralization of this residue (Malinowski & Fridovich, 1979; Cocco et al., 1982; Cudd & Fridovich, 1982; Marmocchi et al., 1982; Borders et al., 1985). Site-directed mutagenesis, less likely to result in steric hindrance, has not been performed on arginine-141 of the bovine enzyme but has been applied to the corresponding arginine-143 of the highly homologous human enzyme (Beyer et al., 1987). Activity measurements on human isoleucine-143 SOD are 11% of wild-type rates at ~0.13 ionic strength, within the range seen with covalently modified bovine SOD's. Our results on 141-neutralized bovine SOD predict five times the activity of the isoleucine-substituted human enzyme at this salt concentration. This discrepancy [as well as the loss of 57% of activity in the charge-conserved lysine-143 human SOD (Beyer et al., 1987)] is most likely due to nonelectrostatic factors associated with structural rearrangements of the active-site channel. A simple explanation is that the approach of superoxide to the copper ion is extremely sensitive to the conformation of the bottom of the channel and any modification of arginine-141 will result in significant steric hindrance. Further possible roles for this residue, such as docking through hydrogen bonding (Getzoff et al., 1983; Osman & Basch, 1984) or a role in a more complex molecular mechanism (Osman & Basch, 1984), may also be involved.

The observed retention of negative salt dependence with bovine SOD covalently modified at arginine-141 (Cudd & Fridovich, 1982) is likely to be characteristic of the charge neutralization itself. The present simulations show that purely electrostatic effects of arginine-141 neutralization result in significant decreases in reaction rates without loss of negative salt dependence, in agreement with the experimental data. Localization of this positive charge's effect within the channel, which has been suggested in other theoretical studies (Getzoff et al., 1983), can explain this behavior. Modification of arginine-141 would greatly influence the probability of reaction once superoxide has enetered the channel but would have a relatively small effect on the salt dependence of diffusion in the bulk solvent.

Lysine-134 is situated at the lip of the active-site channel, about 13 Å from the copper ion, and on the basis of potential maps using simpler electrostatic models has been proposed to play a major role in electrostatic guidance of superoxide into the channel (Getzoff et al., 1983). Our results support this role, with charge neutralization and reversal decreasing reaction rates by 35% and 60%, respectively, at physiological salt. Although modifications to lysine-134 consistently result in less dramatic changes in reaction rate and collision efficiency magnitudes than those seen with arginine-141, salt dependence is seen to be more responsive to changes in the lysine-134 charge. Using rough estimates based on least-squares fitting of the curves in Figure 5b to straight lines, 134-neutralized and negative models exhibit only about 75% and 35% of the salt dependence of the wild-type model, respectively. Although this residue appears to be less essential than arginine-141 for maximal reaction rates, the sensitivity of results to ionic strength suggests that is effect is felt further into the solvent, i.e., during a greater proportion of the diffusion process.

Lysine-120 is also situated at the edge of the channel, about 12 Å from the active-site copper, but on the opposite side from the area around arginine-141 and lysine-134. Modifications at this position cause relatively small effects (~−10% at physiological salt) on both reaction rates and collision efficiencies. Effects on ionic strength are similarly modest. These results are very similar to those obtained when negative point charges are assigned to neutral active-site residues as discussed below. The observed effects upon modification of lysine-120 are consistent with a general facilitory effect of any positive charge in the active-site region and do not indicate any specific role for this residue in the electrostatic steering mechanism.

Modification of Negatively Charged Residues. Although the active-site region of Cu/Zn SOD is predominantly positively charged, the enzyme carries an overall negative charge due to widely scattered anionic residues. To understand the electrostatic control of SOD catalysis, it is important to establish whether these residues contribute to the facilitated diffusion of superoxide into the channel. We have addressed this question by altering the charges associated with three anionic residues, all fairly highly conserved in published Cu/Zn SOD sequences. Glutamate-131 and glutamate-130 are located in the active-site region and have been proposed to play major and minor roles, respectively, in the electrostatic steering process (Getzoff et al., 1983). Aspartate-11, in contrast, is located on the β-barrel portion of the enzyme, fairly distant from both active-site channels. Our results indicate that none of these negative charges function to enhance the electrostatic steering of superoxide into the SOD active site, at least under the steady-state conditions assumed in our simulations. For all three residues, neutralization or reversal of the negative charge produced increased reaction rates (Figure 6a). Although part of this effect is due to increased collision rates accompanying the change in net SOD charge from −4e to −2e or neutrality, collision efficiencies (Figure 6b) are also greater than those of wild type in the modified SOD's.

Modification of glutamate-131, at the lip of the active-site channel, markedly increased magnitudes of both reaction rates and collision efficiencies. A positive charge at this position doubled the predicted reaction rate in comparison to that of wild type at the lowest salt concentration and produced a 50% increase in activity at the highest (Figure 6a). Sharp and co-workers have also reported a large effect upon modification of the glutamate-131 charge; their Brownian dynamics simulation of the 131-neutralized enzyme at zero salt predicted a 75% increase in activity, in agreement with our results on that model extrapolated back to zero. The increases in ionic strength dependence of the reaction rate for 131-modified models (Figure 6a) are largely due to the changes in net charge as reflected in collision rates. The salt dependence of collision efficiencies (Figure 6b) remains about the same as for wild type, even when the charge polarity is reversed. As with the much more deeply situated arginine-141, this may indicate a localization of the residue's electrostatic effect within the channel. Such a localization is plausible since the side chain of glutamate-131 extends into the channel.

Results of modifications to the other two anionic residues are surprisingly similar, given that glutamate-130 is situated next to glutamate-131, also at the lip of the channel but extending into the solvent, while aspartate-11 is located on the

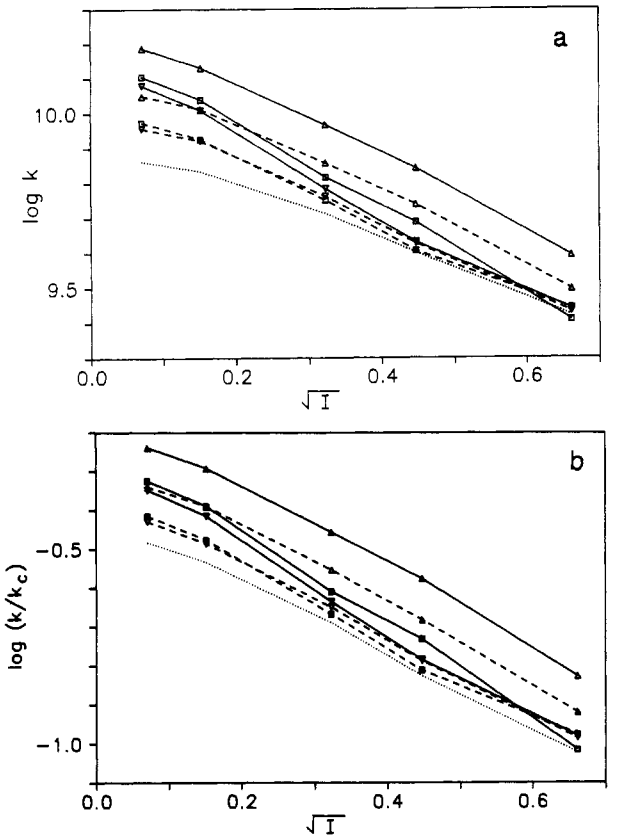

FIGURE 6: Simulations of SOD models with point charge modifications at anionic residues. As in Figure 5, except that modified residues were glutamate-131 (△), glutamate-130 (□), and aspartate-11 (▽).

β-barrel. (The orientation of aspartate-11 relative to the more proximal copper ion of the opposite subunit is illustrated in Figure 2). Effects on reaction rate for the positive charge substitution range from a 70% increase over wild type at the lowest ionic strength to essentially no change at high salt (Figure 6a). Modification of these residues produces increases in the salt dependence of reaction rates, which are only partially attributable to gross collision rates, since collision efficiencies also exhibit increased salt dependence (Figure 6b). This is probably an indication that these residues, which extend into the bulk solvent more than glutamate-131, affect the long-range approach of superoxide to the channel. Alterations in the glutamate-130 charge produce slightly greater effects than those seen with aspartate-11, but in both cases results upon neutralization are comparable to simulations where positive charges are assigned to neutral active-site residues (next section). As in the case of lysine-120, charges at these positions appear to affect electrostatic steering in a general manner that is characteristic of a wide region surrounding the active-site channel.

Modification of Neutral Residues. To further define the electrostatic steering mechanism of SOD, we altered the SOD charge distribution at various neutral residues widely distributed over the enzyme surface. These introduced charges are not expected to reflect specific roles in the SOD steering mechanism, but rather should reveal more general effects of point charge locations. By including residues distant from the active site, we address the proposed electrostatic steering role (Getzoff et al., 1983; Fridovich, 1986) of the repulsive field that surrounds much of the SOD dimer. [Sharp et al. (1987a) have argued against such a role, on the basis of Brownian dynamics simulations of SOD models with only positive (net enzyme = +38e) or negative charges (net charge = −42e) included in the distribution.] Positive and negative charges

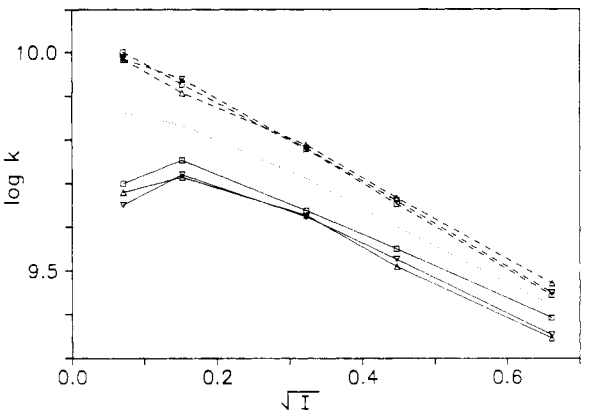

FIGURE 7: Simulations of SOD models with point charge modifications at neutral active-site residues. Dotted line corresponds to bimolecular reaction rate constants for Cu^{2+} SOD from Figure 1. Points indicate simulated reaction rate constants for SOD models with modifications at alanine-138 (△), asparagine-63 (□), and alanine-58 (▽). Either +1 (dashed lines) or −1 (solid lines) units of protonic charge were introduced. Standard deviations (not shown) are approximately equal to those for Cu^{+} SOD in Figure 4.

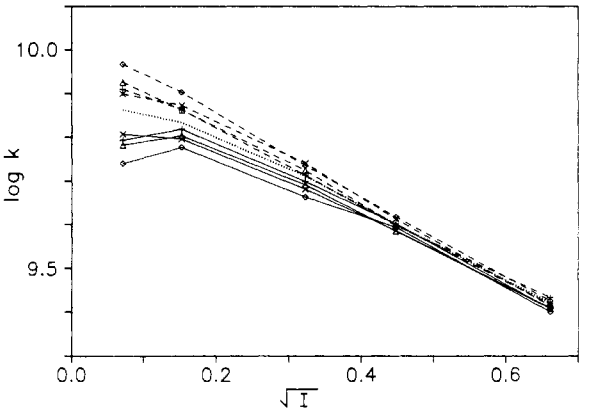

FIGURE 8: Simulations of SOD models with point charge modifications at neutral β-barrel residues. As in Figure 7, except that modified residues were valine-5 (◇), threonine-17 (×), threonine-30 (△), and isoleucine-94 (+).

have been introduced at alanine-58, asparagine-63, and alanine-138 within the active-site region and at valine-5, threonine-17, threonine-30, and isoleucine-94 located progressively further from the copper ion on the β-barrel of the opposite subunit (see Figure 2). The active-site residues and valine-5, at the interface of the two subunits, are highly conserved, while the other β-barrel residues, all facing out into the solvent, show more sequence variability.

Simulation results for the neutral active-site residues are very similar to results seen upon neutralization of lysine-120, glutamate-130, and aspartate-11. We observe a slightly greater effect on magnitude (~15% versus ~10% at physiological salt) and a slightly smaller effect on salt dependence for both reaction rates (Figure 7) and collision efficiencies (data not shown) in comparison to the charged residues. These differences, qualitatively similar to the trend seen with arginine-141, lysine-134, and glutamate-131, are probably due to the slightly more internal location of these neutral residues within the channel.

Introduction of a positive or negative charge at valine-5 results in reaction rates (Figure 8) and collision efficiencies (data not shown) essentially identical with those seen upon neutralization of glutamate-130 and aspartate-11 or lysine-120, respectively. Of the neutral β-barrel residues that we address, this is the nearest to the active-site channel. As the location of the modified residue is moved further from the channel,

effects on the steering mechanism progressively disappear. There is no point at which a negative charge enhances or a positive charge suppresses electrostatic steering through an effect on the negative potential region. For the most distant residue, isoleucine-94, all effects on reaction rates are attributable to the change in net charge as reflected by collision rates; collision efficiencies are indistinguishable from those of wild-type whether a positive or negative charge has been introduced. These results argue against a significant role for SOD's large negative potential region in the electrostatic steering mechanism, at least under steady-state conditions.

Concluding Remarks

These Brownian dynamics simulations on modified SOD models yield an overall picture of the roles of individual point charges in the enzyme's electrostatic steering mechanism. Changes in the charge distribution produce changes in the collision rate for superoxide and the total SOD surface that are completely determined by the net charge on the enzyme. In contrast, the collision efficiency, the ratio of effective to total collisions, does vary widely with the location of the modified charge. Charges within the channel can affect collision efficiencies to a great degree but, apparently due to localization of their influence, have little effect on the salt dependence of the reaction. Maximum effects, seen upon charge reversal at arginine-141 and at glutamate-131, amount to 75% of wild-type rates at physiological salt. A different pattern is seen with charges outside the channel. Within a wide region surrounding the active site, alterations by a unit of protonic charge produce only $\sim$10% enhancement or suppression of activity at physiological salt but do change salt dependence, indicating that these charges are felt in the bulk solvent. This pattern extends to residues on the proximal part of the β-barrel of the opposite subunit. As modifications are made to more distant residues, however, all effects on the steering mechanism disappear and only net charge effects on the total collision rate remain.

It has been suggested that both the extensive region of negative potential that surrounds much of the SOD dimer (Getzoff et al., 1983; Fridovich, 1986) and specific anionic residues (Getzoff et al., 1983) function in steering superoxide away from the general enzyme surface and into the active-site channel. If this were the case, point charge alterations disrupting or enhancing such function should have effects opposite to alterations affecting the positive potential of the active-site channel. In fact, no enhancement of the steering mechanism by a negative charge or suppression by a positive charge is observed for the wide range of residues that we have investigated. There appear to be no general or specific roles for anionic residues in the electrostatic facilitation of superoxide diffusion to the SOD active site under the steady-state conditions assumed in our simulations. The steepness of the electrostatic potential gradient due to the presence of anionic residues may, however, accelerate the approach to steady state and thus be important to the functioning of SOD in vivo, where superoxide levels can fluctuate rapidly (Bannister et al., 1987). Other possible functions for these negative surface charges include structural roles and prevention of superoxide encounter at sensitive points on the SOD surface.

Because SOD exhibits diffusion-controlled catalysis, an obvious approach to design of a more efficient enzyme is enhancement of the steering mechanism through site-directed mutagenesis involving charged residues. Unfortunately, we find the modifications of the charge distribution usually result in only modest effects on reaction rates. Significant enhancement of activity is observed upon alteration of glutamate-131, but this is a conserved active-site residue that may be involved in a salt bridge with lysine-134 (Tainer et al., 1982) and essential to the integrity of channel. Recent studies on human SOD with an active-site residue, threonine-136, substituted by isoleucine (Bertini, 1989) suggest that the active-site region can undergo quite large structural changes without loss of activity. We plan an approach combining molecular dynamics and Brownian dynamics simulations to study effects of residue, rather than simple charge, modifications within the tightly enclosed active-site channel of SOD. However, the only practical approach for increasing SOD activity may turn out to be multiple substitutions involving charged resiues. We plan to address the electrostatic effects of multiple point charge modifications in a future paper.

References

Allison, S. A., & McCammon, J. A. (1985) *J. Phys. Chem. 89*, 1072–1074.

Allison, S. A., Ganti, G., & McCammon, J. A. (1985) *Biopolymers 24*, 1323–1336.

Allison, S. A., Northup, S. H., & McCammon, J. A. (1986) *Biophys. J. 49*, 167–175.

Allison, S. A., Bacquet, R. J., & McCammon, J. A. (1988) *Biopolymers 27*, 251–269.

Allison, S. A., Sines, J. J., & Wierzbicki, A. (1989) *J. Phys. Chem. 93*, 5819–5823.

Argese, E., Viglino, P., Rotilio, G., Scarpa, M., & Rigo, A. (1987) *Biochemistry 26*, 3224–3228.

Bannister, J. V., Bannister, W. H., & Rotilio, G. (1987) *CRC Crit. Rev. Biochem. 22*, 111–180.

Bertini, I., Banci, L., Luchinat, C., Bielski, B. H. J., Cabelli, D. E., Mullenbach, G. T., & Hallewell, R. A. (1989) *J. Am. Chem. Soc. 111*, 714–719.

Beyer, W. F., Jr., Fridovich, I., Mullenbach, G. T., & Hallewell, R. (1987) *J. Biol. Chem. 262*, 11182–11187.

Borders, C. L., Jr., Saunders, J. E., Blech, D. M., & Fridovich, I. (1985) *Biochem. J. 230*, 771–776.

Case, D. A. (1988) *Prog. Biophys. Mol. Biol. 52*, 39–70.

Cass, A. E. G., Hill, H. A. O., Smith, B. E., Bannister, J. V., & Bannister, W. H. (1977) *Biochemistry 16*, 3061–3066.

Cocco, D., Rossi, L., Barra, D., & Rotilio, G. (1982) *FEBS Lett. 150*, 303–306.

Cudd, A., & Fridovich, I. (1982) *J. Biol. Chem. 257*, 11443–11447.

Davis, M., & McCammon, J. A. (1990) *Chem. Rev. 90*, 509–521.

Debye, P. (1942) *Trans. Electrochem. Soc. 82*, 265–272.

Desideri, A., Falconi, M., Parisi, V., Morante, S., & Rotilio, G. (1988) *Free Radical Biol. Med. 5*, 313–317.

Dickerson, R. E. (1969) *Molecular Thermodynamics*, W. A. Benjamin, Inc., New York.

Edmonds, D. T., Rogers, N. K., & Sternberg, M. J. E. (1984) *Mol. Phys. 52*, 1487–1494.

Fielden, E. M., Roberts, P. B., Bray, R. C., Lowe, D. J., Mautner, G. N., Rotilio, G., & Calabrese, L. (1974) *Biochem. J. 139*, 499.

Fridovich, I. (1986) *Adv. Enzymol. Relat. Areas Mol. Biol. 58*, 61–97.

Ganti, J. A., McCammon, J. A., & Allison, S. A. (1985) *J. Phys. Chem. 89*, 3899–3902.

Getzoff, E. D., Tainer, J. A., Stempien, M. M., Bell, G. I., & Hallewell, R. A. (1989) *Proteins: Struct., Funct., Genet.* (in press).

Getzoff, E. D., Tainer, J. A., Weiner, P. K., Kollman, P. A., Richardson, J. S., & Richardson, D. C. (1983) *Nature 306*, 287–290.

Halliwell, B., & Gutteridge, J. M. C. (1984) *Biochem. J. 219*, 1-14.
Head-Gordon, T., & Brooks, C. L. (1987) *J. Phys. Chem. 91*, 3342-3349.
Hjalmarsson, K., Marklund, S. F., Engström, Å, & Edlund, T. (1987) *Proc. Natl. Acad. Sci. U.S.A. 84*, 6340-6344.
Hodgson, E. K., & Fridovich, I. (1975) *Biochemistry 14*, 5299-5303.
Jayaram, B., Sharp, K., & Honig, B. H. (1989) *Biopolymers 28*, 975-993.
Klapper, I., Hastrom, R., Fine, R., Sharp, K., & Honig, B. (1986) *Protein 1*, 47-59.
Klug-Roth, D., Fridovich, I., & Rabani, J. (1973) *J. Am. Chem. Soc. 95*, 2786.
Koppenol, W. H. (1981) in *Oxygen and Oxy-Radicals in Chemistry and Biology* (Rodgers, M. A., & Powers, E. L., Eds.) pp 671-674, Academic Press, New York.
Malinowski, D. P., & Fridovich, I. (1979) *Biochemistry 18*, 5909-5917.
Marmocchi, F., Mavelli, I., Rigo, A., & Rotilio, G. (1982) *Biochemistry 21*, 2853-2856.
Matthews, B. W. (1987) *Biochemistry 26*, 6885-6888.
McAdam, M. E., Fielden, E. M., Lavelle, F., Calabrese, L., Cocco, D., & Rotilio, G. (1977) *Biochem. J. 167*, 271-274.
Neumann, E. (1981) in *Structural and Functional Aspects of Enzyme Catalysis* (Eggerer, H., & Huber, R., Eds.) pp 45-58, Springer, Berlin.
Northrup, S. H., & Hynes, J. T. (1979) *J. Chem. Phys. 71*, 871-883.
Northrup, S. H., Allison, S. A., & McCammon, J. A. (1984) *J. Chem. Phys. 80*, 1517-1524.
O'Neill, P., Davies, S., Fielden, E. M., Calabrese, L., Capo, C., Marmocchi, F., Natoli, G., & Rotilio, G. (1988) *Biochem. J. 251*, 41-46.
Osman, R., & Basch, H. (1984) *J. Am. Chem. Soc. 106*, 5710-5714.
Rigo, A., Viglino, P., Rotilio, G., & Tomat, R. (1975) *FEBS Lett. 50*, 86-88.
Rogers, N. K., & Sternberg, M. J. E. (1984) *J. Mol. Biol. 174*, 527-542.
Sharp, K., Fine, R., & Honig, B. (1987a) *Science 236*, 1460-1463.
Sharp, K., Fine, R., Schulten, K., & Honig, B. H. (1987b) *J. Phys. Chem. 91*, 3624-3631.
Sines, J., Allison, S. A., Wierzbicki, A., & McCammon, J. A. (1990) *J. Phys. Chem. 94*, 959-961.
Tainer, J. A., Getzoff, E. D., Beem, K. M., Richardson, J. S., & Richardson, D. C. (1982) *J. Mol. Biol. 160*, 187-217.
Warwicker, J., & Watson, H. C. (1982) *J. Mol. Biol. 157*, 671-679.

Interaction of Factor Xa with Heparin Does Not Contribute to the Inhibition of Factor Xa by Antithrombin III-Heparin†

Barbara A. Owen* and Whyte G. Owen

Section of Hematology Research and Departments of Biochemistry and Molecular Biology, Mayo Clinic and Foundation, Rochester, Minnesota 55905

Received March 29, 1990; Revised Manuscript Received June 21, 1990

ABSTRACT: Factor Xa modified by reductive methylation (>92%) loses the capacity to bind heparin as determined both by gel chromatography and by sedimentation equilibrium ultracentrifugation. The kinetic properties of methylated factor Xa differ, with respect to K_M and V_{max} for a synthetic tripeptide substrate and for antithrombin III inhibition rate constants, from those of the unmodified enzyme. The 10000-fold rate enhancement elicited by the addition of heparin to the antithrombin III inhibition reaction, however, is the same. The observed second-order rate constants (k''_{obs}) for antithrombin III inhibition of factor Xa and methylated factor Xa are 3000 and 340 M^{-1} s^{-1}, respectively, whereas k''_{obs} values for the inhibition of factor Xa or methylated factor Xa with antithrombin III-heparin are 4×10^7 and 3×10^6 M^{-1} s^{-1}, respectively. These findings provide direct evidence that the interaction of factor Xa with heparin is not involved in the heparin-enhanced inhibition of this enzyme.

Heparin is a sulfated glycosaminoglycan found in the basophilic granules of mast cells and various mammalian tissue (Jorpes et al., 1937; Nader & Dietrich, 1989). The degree and type of sulfation and oligosaccharide sequence and length are determinants for binding to the glycoprotein antithrombin III (Andersson et al., 1976; Atha et al., 1985; Lindahl et al., 1980), a member of the serpin superfamily of protease inhibitors. Complement C1s, trypsin, plasmin, kallikrein, and the clotting factors XIIa, XIa, Xa, IXa, and thrombin are inhibited by antithrombin III via the formation of a stable covalent bond between the inhibitor and the active site of the enzyme (Rosenberg & Damus, 1973). Heparin bound to antithrombin III increases the rate of inhibition by as much as 50000-fold in the case of thrombin and to variable, but smaller degrees, for the other enzymes (Ogston et al., 1976; Rosenberg, 1977; Jordan et al., 1980; Holyaerts et al., 1984).

The mechanism of the rate enhancement induced by heparin has proven problematic; inherent in this system is the difficulty in attributing either heparin-inhibitor or heparin-protease interactions to change in the rate of inhibition. Substantial evidence indicates a requirement for both interactions for the

†Supported by Grant PO1-HL-17430 from the National Heart, Lung and Blood Institute.

0006-2960/90/0429-9412$02.50/0